

CCEM Technical Report of Pilot Study on Dielectric Material Measurement

Yuto Kato¹, Tae-Weon Kang², Hyunji Koo², Djamel Allal³, Hao Xu⁴, and Yusong Meng⁵

¹National Metrology Institute of Japan (NMIJ), National Institute of Advanced Industrial Science and Technology, Japan

²Division of Physical Metrology, Korea Research Institute of Standards and Science (KRISS), Korea

³Electrical Metrology / Scientific and Industrial Metrology, Laboratoire National de Métrologie et d'Essais (LNE), France

⁴Information and Electronic Division, National Institute of Metrology (NIM), China

⁵National Metrology Centre (NMC), Agency for Science, Technology and Research (A*STAR), Singapore

Version 4, May 31, 2023

Contents

- 1 Introduction
- 2 Participants
- 3 Traveling standards
- 4 Comparison pattern
- 5 Transmission/reflection method
 - 5.1 Comparison protocol
 - 5.2 Measurement systems of participating laboratories
 - 5.3 Results
 - 5.4 Discussions
- 6 Resonator method
 - 6.1 Comparison protocol
 - 6.2 Measurement systems of participating laboratories
 - 6.3 Results
 - 6.4 Discussions
- 7 Conclusions
- 8 References

1 Introduction

The accurate measurement of complex permittivity is essential in the design of electromagnetic components and devices. Permittivity measurements at millimeter frequencies are becoming increasingly important with the growing demand for millimeter-wave applications, including automotive radars and 5G/6G wireless communications. The measurement methods of the complex permittivity at microwave and millimeter-wave bands can be classified into two categories: the transmission/reflection (T/R) and resonator methods, which can be used to characterize high-loss and low-loss materials, respectively [1-5]. Various measurement systems have been proposed for both T/R and resonator methods. It is critical for the industries and academia involved in the development of materials, components, and devices for electromagnetic applications to verify the consistency of permittivity measurements obtained from different systems.

It is a function of the Mutual Recognition Arrangement (MRA) of the Bureau International des Poids et Mesures (BIPM) that the equivalence of signatory National Metrology Institutes' (NMI) standards should be established by means of international comparison exercises. To establish such equivalence in permittivity measurement, it was decided to initiate a CCEM Pilot Study on the permittivity of dielectric materials. In the pilot study, the measurement results obtained independently at each participating laboratory were summarized and compared. One type of high-loss material and three types of low-loss materials were prepared as traveling samples, sent to the participants, and characterized by T/R and resonator methods, respectively. Some laboratories only participated in the comparison of high-loss material characterization.

2 Participants

This report summarizes and compares the permittivity measurement results of the following participating laboratories:

- Korea Research Institute of Standards and Science (KRISS, Korea)
- Laboratoire National de Métrologie et d'Essais (LNE, France)
- National Institute of Metrology (NIM, China)
- National Metrology Centre, Agency for Science, Technology and Research (NMC, A*STAR, Singapore)
- National Metrology Institute of Japan (NMIJ, Japan)

Table 1 summarizes the participation items and measurement methods of each participating laboratory.

Table 1: Participation items and measurement methods of each participating laboratory

Laboratory	High-loss material characterization		Low-loss material characterization	
	Participation	Method	Participation	Method
KRISS	Yes	Waveguide T/R method	Yes	Split cylinder resonator method
LNE			No	—
NIM			Yes	Split cylinder resonator method
NMC, A*STAR			No	—
NMIJ (Pilot)			Yes	Split cylinder resonator method, Balanced-type circular disk resonator method

3 Traveling standards

In the comparison, one type of high-loss material and three types of low-loss materials, all of which were machined from commercially available materials, were prepared as traveling samples. One high-loss material sample was precisely machined into rectangular cuboids such that it tightly fits into an aperture of a WR-90 waveguide and measured by using a waveguide T/R method. Three low-loss material samples were prepared with sheets and measured using resonator methods applicable to sheet samples.

The details of the prepared sample set are summarized in Table 2, where “XXX” denotes the abbreviation of each participating laboratory. Four sets of samples were prepared for participating laboratories except for the pilot laboratory, NMIJ, which measured all samples sent to the other four laboratories before sending and after returning. Only acrylic samples (MAT.TR-XXX) were prepared for laboratories participating exclusively in high-loss material characterization (LNE and NMC). Each acrylic sample was inserted into a waveguide fixture with the specifications shown in Table 3, and not removed from the fixture during the comparison. Table 4 presents the samples and corresponding measurement methods. In Table 4, the measured frequencies of the comparison are also presented. Photographs of the traveling samples are shown in Fig. 1.

Table 2: Details of the traveling samples

Identifier	Material	Manufacturer	Nominal values[mm]		No. of pcs
			Width×Length	Thickness	
MAT.TR-XXX	Acrylic	Mitsubishi Chemical	22.86×10.16	5.0	1
MAT.RES1-XXX	Cyclo olefin polymer (COP)	Zeon	50×50	0.25	2
MAT.RES2-XXX	Silica glass	Asahi Glass	50×40	0.30	2
MAT.RES3-XXX	Alkali-free glass	Asahi Glass	50×40	0.31	2

Table 3: Details of the traveling fixture

Identifier	Nominal values[mm]		No. of pcs
	Aperture size	Length	
FIX.TR-XXX	22.86×10.16	9.78	1

Table 4: Measurement method and frequency for each traveling sample

Identifier	Measurement method	Frequency
MAT.TR-XXX	Waveguide T/R method	From 8 GHz to 12 GHz (inclusive) in 100 MHz steps
MAT.RES1-XXX	Resonator method	At least at one frequency point within 20-60 GHz
MAT.RES2-XXX		
MAT.RES3-XXX		

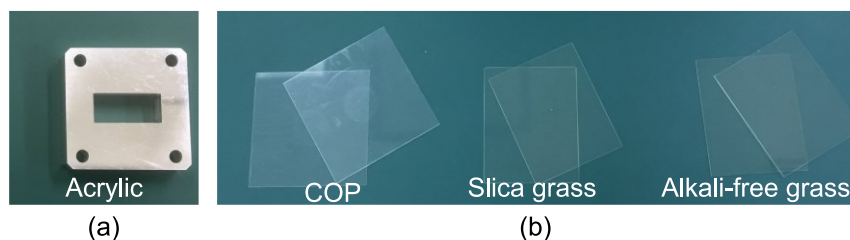


Fig.1 (a) Traveling sample for T/R method with fixture. (b) Traveling samples for resonator method.

4 Comparison pattern

The traveling samples of all the participating laboratories were measured first by the pilot laboratory, then sent to each participating laboratory. Each laboratory returned the samples to the pilot laboratory after the completion of their measurements. Finally, the pilot laboratory remeasured all the returned samples to ensure that the electrical characteristics of the items remained essentially the same. The timeline of the comparison is presented in Table 5.

Table 5: Timeline of the comparison

	2017	2018	2019	2020	2021
NMIJ	Prepare and measure samples →	Send samples to participating laboratories (Dec. 2017)			Remeasure samples and prepare report →
KRISS		Measure samples and prepare report ←→	Complete sample return and report submission to NMIJ (Dec. 2018)		
LNE		Measure samples and prepare report ←→	Complete sample return and report submission to NMIJ (Feb. 2019)		
NIM		Measure samples and prepare report ←→	Complete sample return and report submission to NMIJ (Nov. 2018)		
NMC, A*STAR		Measure samples and prepare report ←→			Complete sample return and report submission to NMIJ (Mar. 2021)

5 Transmission/reflection method

5.1 Comparison protocol

The acrylic samples were prepared for material characterization based on the waveguide T/R method (MAT.TR-XXX). To avoid scratching the sample when inserting it into the fixture, the sample was sent to each laboratory after being inserted into the WR-90 waveguide fixture at NMIJ. The sample was inserted into the fixture such that one sample interface is coincident with an end face of the fixture (see Fig. 2). The sample was measured from 8 GHz to 12 GHz (inclusive) in 100 MHz steps. Among all frequency points, the measurement results of the complex permittivity at 8 GHz, 10 GHz, and 12 GHz obtained at the participating laboratories were compared to analyze the degree of equivalence (DoE) of the measurements. The sample thickness and fixture length measured at NMIJ were provided to the participating laboratories to calculate the complex permittivity from the measured S-parameters. The details of the measurement systems of the participating laboratories are described in Section 5.2. The general information on the waveguide T/R method is described as follows [1].

For the sample and fixture used in the comparison (see Fig. 2), the S-parameters at the fixture interfaces are written as

$$\begin{aligned}
 S_{11} &= \frac{\Gamma(1 - z^2)}{1 - \Gamma^2 z^2}, & S_{22} &= \exp\{-2\gamma_0(L - d)\} \frac{\Gamma(1 - z^2)}{1 - \Gamma^2 z^2}, \\
 S_{21} &= S_{12} = \exp\{-\gamma_0(L - d)\} \frac{z(1 - \Gamma^2)}{1 - \Gamma^2 z^2},
 \end{aligned} \tag{1}$$

where $z = \exp(-\gamma d)$, d is the sample thickness, $\Gamma = (\gamma_0 - \gamma)/(\gamma_0 + \gamma)$ is the reflection coefficient at the sample interface, and γ_0 and γ are propagation constants in the air and sample regions, respectively, given by

$$\gamma_0 = j \frac{\omega}{c} \sqrt{\epsilon_a - \left(\frac{\omega_c}{\omega}\right)^2}, \quad \gamma = j \frac{\omega}{c} \sqrt{\epsilon_r^* - \left(\frac{\omega_c}{\omega}\right)^2}, \quad (2)$$

where ω is the angular frequency, $c = 299,792,458$ m/s is the speed of light, $\epsilon_a = 1.000649$ is the relative permittivity of 'standard' air at a temperature of 23 °C, 50 % relative humidity, and 1013.25 hPa atmospheric pressure, and $\epsilon_r^* = \epsilon_r' - j\epsilon_r''$ is the complex relative permittivity of the sample. The sample permittivity can be determined from the measured S-parameters, sample thickness, and fixture length using Eq. (1) and (2), where the comparison parameters between the participating laboratories were the relative permittivity ϵ_r' and loss tangent $\tan \delta = \epsilon_r''/\epsilon_r'$.

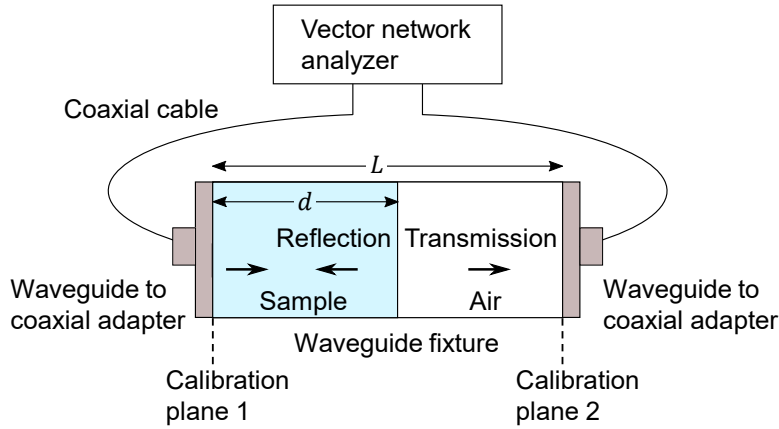


Fig. 2 Schematic of a measurement system of waveguide T/R method.

5.2 Measurement systems of participating laboratories

(1) KRISS

The S-parameters of the fixture with the sample inserted were obtained by using a vector network analyser (VNA), and calculated its relative permittivity using the following equation:

$$S_{21}S_{12} - S_{11}S_{22} = \exp\{-2\gamma_0(L - d)\} \frac{z(1 - \Gamma^2)}{1 - \Gamma^2 z^2}. \quad (3)$$

The VNA was calibrated by the through-reflect-line (TRL) calibration method. The data of the thicknesses of the sample and the fixture were measured and provided by the pilot laboratory.

The measurement conditions were as follows:

- Temperature: (23.0 ± 0.5) °C

- Relative humidity: (50 ± 10) %

The uncertainty was estimated using the following equations:

$$u^2(\epsilon'_r) = \sum_{i,j} \left\{ \left(\frac{\partial \epsilon'_r}{\partial |S_{ij}|} \right)^2 u^2(|S_{ij}|) + \left(\frac{\partial \epsilon'_r}{\partial \theta_{ij}} \right)^2 u^2(\theta_{ij}) \right\} + \left(\frac{\partial \epsilon'_r}{\partial d} \right)^2 u^2(d) + \left(\frac{\partial \epsilon'_r}{\partial L} \right)^2 u^2(L) + u_{w_{\text{eff}}}^2(\epsilon'_r) \quad (4)$$

$$u^2(\epsilon''_r) = \sum_{i,j} \left\{ \left(\frac{\partial \epsilon''_r}{\partial |S_{ij}|} \right)^2 u^2(|S_{ij}|) + \left(\frac{\partial \epsilon''_r}{\partial \theta_{ij}} \right)^2 u^2(\theta_{ij}) \right\} + \left(\frac{\partial \epsilon''_r}{\partial d} \right)^2 u^2(d) + \left(\frac{\partial \epsilon''_r}{\partial L} \right)^2 u^2(L) + u_{w_{\text{eff}}}^2(\epsilon''_r) \quad (5)$$

$$w_{\text{eff}} = w - \frac{(4 - \pi)r^2}{h} \quad (6)$$

$$u^2(\tan \delta) = \left(-\frac{\epsilon_i}{(\epsilon_r)^2} \right)^2 u(\epsilon_r)^2 + \left(\frac{1}{\epsilon_r} \right)^2 u(\epsilon_i)^2 \quad (7)$$

where w , h , and r are the width, height and roundness of the corners of the waveguide aperture, respectively. w_{eff} is the effective waveguide width. The partial derivatives are calculated from Eq. (3) using the same method as the one presented in [6]. The Monte Carlo (MC) simulations were also used to evaluate the uncertainty due to w and h . The S-parameters uncertainty ($u(|S_{ij}|)$, $u(\theta_{ij})$, $i, j = 1, 2$) includes the VNA system performances, VNA residual errors, random errors in the VNA system, and the repeatability. The dimensions of the fixture and sample and associated uncertainties are shown in Table 6.

Table 6: Dimension and the uncertainty ($k = 1$) of the fixture and the sample at KRISS

Parameters	d	L	w	h	r
Measured value (mm)	4.9543	9.7943	22.86	10.16	0.01
Uncertainty (mm)	0.84e-3 ⁽¹⁾	1.1e-3 ⁽¹⁾	±0.01 ⁽²⁾	±0.01 ⁽²⁾	-

(1) The values provided by NMIJ.

(2) Tolerance given by the manufacturer.

(2) LNE

The relative permittivity and the loss tangent have been derived from S parameters measured with a VNA, the dimensions (length and width) of the waveguide fixture and the thickness of the material under test (acrylic).

The S parameter data are based on 2 repeated calibrations at the waveguide reference plane and 2 measurements per calibration. The uncertainties of S parameters are based on LNE's calibration capabilities.

The dimensions and their uncertainties used are those provided by the pilot laboratory. A second determination carried out using the dimensions measured in our laboratory show a negligible and a very small deviation with regard to the expanded uncertainty, for the relative permittivity and the loss tangent, respectively.

The complex permittivity is obtained using the T/R Nicolson–Ross–Weir-based material parameter

extraction method and by considering a known value for the complex permeability ($\mu_r^* = 1$).

The uncertainties were propagated from dimensional and S parameter data to the measurands using a Monte Carlo method.

LNE establishes the permittivity traceability through the traceability of impedance measurements and length measurements, to the SI meter.

(3) NIM

Based on the T/R method, the X-band measurement system for characterizing the complex permittivity of materials was developed by using the waveguide fixture, as shown in Fig. 3. The S-parameters of the fixture holding the sample were measured from 8 GHz to 12 GHz in 100 MHz steps. The TRL calibration was used before each measurement. The complex permittivity at each frequency point was calculated from the measured S-parameters, sample thickness and fixture length by using an iterative method. In evaluating the measurement uncertainties of ϵ_r' and $\tan \delta$, the uncertainties of S-parameters and dimensions of the sample and fixture were considered. The total uncertainties were calculated by a well-established differential uncertainty analysis. The traceability route of the measurement was shown in Fig. 4.

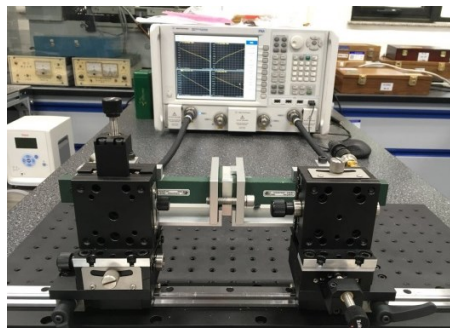


Fig.3 The X-band measurement system based on the waveguide fixture at NIM

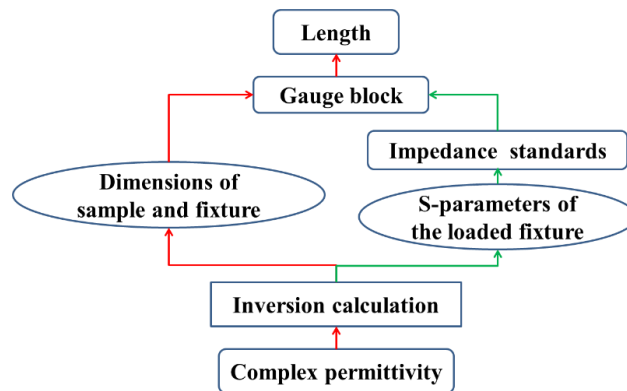


Fig.4 The traceability route of the T/R method at NIM

(4) NMC, A*STAR

The measurement setup at NMC is the same as the waveguide T/R method schematically shown in Fig. 2. The measurement steps conform to ASTM D5568-14: Standard test method for measuring relative complex permittivity and relative magnetic permeability of solid materials at microwave frequencies using waveguide. In calculating the complex permittivity, the Nicolson-Ross-Weir (NRW) algorithm was used.

The measurements are traceable to NMC’s VNA system (S-parameter which is traceable to impedance standard) and the length standards such as the dimensions of the sample and fixture measured by the pilot laboratory, NMIJ.

(5) NMIJ

The waveguide fixture was connected to a VNA with coaxial-to-waveguide adapters (Keysight technologies, X281C) and coaxial cables, and the S-parameters at the fixture interfaces were measured from 8 GHz to 12 GHz in 100 MHz steps. The sample permittivity was calculated from the measured S-parameters and dimensions of the fixture and sample by iteratively solving Eq. (3), where the initial value for the iterative calculations was obtained from the NRW algorithm.

The measurement uncertainties of ϵ_r' and $\tan \delta$ were evaluated by considering the uncertainty propagations of S-parameters and those of the dimensions of the sample and fixture based on a Monte Carlo analysis. NMIJ establishes the permittivity traceability through the traceability of S-parameter and length measurements, to the SI units (see Fig. 5) [6].

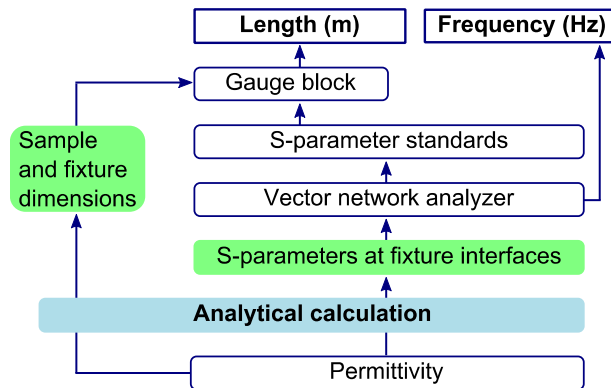


Fig.5 The traceability route of the T/R method at NMIJ

5.3 Results

The measurement results obtained at KRISS, LNE, NIM, and NMC are shown in Tables 7—10, respectively. Tables 11—14 show the measured results of the four samples sent to the four laboratories obtained at NMIJ before sending and after returning. Measurement uncertainties in the tables are the expanded values with a coverage factor $k = 2$. From KRISS, uncertainty budgets were provided as shown in Tables 15—23. Fig. 6 shows a comparison of the measurement results of each sample. For clarity, the uncertainties in Fig. 6 are shown with error bars only at 8 GHz, 10 GHz, and 12 GHz. Fig. 7 summarizes the results and uncertainties at 8 GHz, 10 GHz, and 12 GHz obtained at all the participating laboratories.

Table 7: Measurement results of the relative permittivity and loss tangent of MAT.TR-KRISS (Acrylic) obtained at KRISS

Frequency (GHz)	ϵ_r	$U(\epsilon_r)$	$\tan \delta$	$U(\tan \delta)$
8	2.645	0.027	0.0081	0.0082

8.1	2.645	0.027	0.0081	0.0081
8.2	2.645	0.026	0.0081	0.0081
8.3	2.645	0.026	0.0081	0.0081
8.4	2.645	0.026	0.0081	0.0080
8.5	2.645	0.026	0.0081	0.0080
8.6	2.645	0.026	0.0081	0.0079
8.7	2.644	0.026	0.0081	0.0079
8.8	2.644	0.026	0.0081	0.0079
8.9	2.644	0.026	0.0081	0.0078
9	2.644	0.026	0.0081	0.0078
9.1	2.644	0.026	0.0081	0.0078
9.2	2.644	0.026	0.0081	0.0077
9.3	2.644	0.026	0.0082	0.0077
9.4	2.643	0.026	0.0082	0.0076
9.5	2.643	0.026	0.0082	0.0076
9.6	2.643	0.026	0.0082	0.0076
9.7	2.643	0.026	0.0082	0.0075
9.8	2.643	0.026	0.0082	0.0075
9.9	2.643	0.026	0.0082	0.0074
10	2.643	0.026	0.0082	0.0074
10.1	2.643	0.026	0.0082	0.0074
10.2	2.643	0.026	0.0082	0.0074
10.3	2.642	0.026	0.0082	0.0073
10.4	2.642	0.026	0.0082	0.0073
10.5	2.643	0.026	0.0082	0.0072
10.6	2.643	0.025	0.0084	0.0072
10.7	2.640	0.025	0.0092	0.0071
10.8	2.641	0.025	0.0083	0.0071
10.9	2.641	0.025	0.0082	0.0070
11	2.641	0.025	0.0082	0.0069
11.1	2.641	0.025	0.0082	0.0069
11.2	2.641	0.025	0.0082	0.0068
11.3	2.641	0.025	0.0082	0.0067
11.4	2.641	0.024	0.0082	0.0067
11.5	2.641	0.024	0.0082	0.0066
11.6	2.641	0.024	0.0082	0.0065
11.7	2.641	0.024	0.0083	0.0065
11.8	2.640	0.024	0.0084	0.0064
11.9	2.641	0.024	0.0082	0.0063
12	2.641	0.023	0.0082	0.0062

Table 8: Measurement results of the relative permittivity and loss tangent of MAT.TR-LNE (Acrylic) obtained at LNE

Frequency (GHz)	ϵ_r	$U(\epsilon_r)$	$\tan \delta$	$U(\tan \delta)$
8	2.628	0.081	0.0090	0.0310
8.1	2.632	0.080	0.0100	0.0310
8.2	2.635	0.078	0.0120	0.0300
8.3	2.633	0.077	0.0080	0.0300
8.4	2.631	0.076	0.0100	0.0290
8.5	2.637	0.076	0.0110	0.0290

CCEM Pilot Study Technical Report
Dielectric Material Measurement Pilot Study

8.6	2.638	0.075	0.0120	0.0290
8.7	2.640	0.074	0.0120	0.0280
8.8	2.636	0.073	0.0100	0.0280
8.9	2.636	0.072	0.0110	0.0280
9	2.638	0.072	0.0100	0.0270
9.1	2.636	0.071	0.0120	0.0270
9.2	2.640	0.070	0.0120	0.0270
9.3	2.633	0.070	0.0110	0.0270
9.4	2.632	0.069	0.0120	0.0270
9.5	2.634	0.069	0.0090	0.0270
9.6	2.633	0.069	0.0110	0.0270
9.7	2.636	0.069	0.0120	0.0260
9.8	2.629	0.068	0.0110	0.0260
9.9	2.627	0.068	0.0120	0.0260
10	2.626	0.067	0.0100	0.0260
10.1	2.626	0.067	0.0090	0.0260
10.2	2.633	0.068	0.0090	0.0260
10.3	2.627	0.067	0.0100	0.0260
10.4	2.627	0.067	0.0110	0.0260
10.5	2.622	0.067	0.0100	0.0260
10.6	2.617	0.067	0.0100	0.0260
10.7	2.618	0.067	0.0090	0.0260
10.8	2.620	0.067	0.0080	0.0260
10.9	2.621	0.067	0.0100	0.0260
11	2.620	0.068	0.0110	0.0260
11.1	2.617	0.068	0.0130	0.0260
11.2	2.613	0.067	0.0120	0.0260
11.3	2.610	0.068	0.0100	0.0260
11.4	2.612	0.068	0.0090	0.0260
11.5	2.612	0.068	0.0100	0.0260
11.6	2.612	0.069	0.0110	0.0270
11.7	2.609	0.069	0.0120	0.0270
11.8	2.596	0.068	0.0160	0.0270
11.9	2.610	0.070	0.0130	0.0270
12	2.609	0.070	0.0120	0.0270

Table 9: Measurement results of the relative permittivity and loss tangent of MAT.TR-NIM (Acrylic) obtained at NIM

Frequency (GHz)	ϵ_r	$U(\epsilon_r)$	$\tan \delta$	$U(\tan \delta)$
8	2.608	0.021	0.0056	0.0061
8.1	2.609	0.021	0.0058	0.0061
8.2	2.609	0.021	0.0059	0.0061
8.3	2.609	0.021	0.0058	0.0061
8.4	2.609	0.021	0.0058	0.0062
8.5	2.609	0.021	0.0059	0.0062
8.6	2.608	0.021	0.0059	0.0062
8.7	2.609	0.021	0.0057	0.0062
8.8	2.610	0.021	0.0058	0.0062
8.9	2.609	0.021	0.0060	0.0062
9	2.609	0.021	0.0059	0.0062
9.1	2.610	0.021	0.0060	0.0063
9.2	2.609	0.021	0.0059	0.0063
9.3	2.608	0.021	0.0057	0.0063
9.4	2.609	0.021	0.0058	0.0063
9.5	2.610	0.021	0.0059	0.0063
9.6	2.609	0.021	0.0057	0.0063
9.7	2.609	0.021	0.0056	0.0063
9.8	2.610	0.021	0.0058	0.0063
9.9	2.610	0.022	0.0060	0.0063
10	2.609	0.022	0.0059	0.0063
10.1	2.609	0.022	0.0057	0.0063
10.2	2.609	0.022	0.0056	0.0063
10.3	2.609	0.022	0.0058	0.0063
10.4	2.609	0.022	0.0058	0.0063
10.5	2.610	0.022	0.0058	0.0063
10.6	2.611	0.022	0.0057	0.0063
10.7	2.611	0.022	0.0059	0.0063
10.8	2.609	0.022	0.0060	0.0064
10.9	2.607	0.022	0.0059	0.0063
11	2.608	0.023	0.0058	0.0063
11.1	2.607	0.023	0.0060	0.0063
11.2	2.608	0.023	0.0059	0.0063
11.3	2.609	0.023	0.0059	0.0063
11.4	2.610	0.023	0.0059	0.0062
11.5	2.609	0.023	0.0059	0.0062
11.6	2.608	0.023	0.0058	0.0062
11.7	2.609	0.023	0.0058	0.0062
11.8	2.610	0.023	0.0057	0.0062
11.9	2.608	0.024	0.0057	0.0061
12	2.610	0.024	0.0059	0.0061

Table 10: Measurement results of the relative permittivity and loss tangent of MAT.TR-NMC (Acrylic) obtained at NMC

Frequency (GHz)	ϵ_r	$U(\epsilon_r)$	$\tan \delta$	$U(\tan \delta)$
8	2.646	0.038	0.0082	0.0040
8.1	2.647	0.036	0.0084	0.0039
8.2	2.648	0.035	0.0085	0.0037
8.3	2.649	0.032	0.0086	0.0025
8.4	2.649	0.029	0.0087	0.0027
8.5	2.649	0.029	0.0087	0.0030
8.6	2.650	0.030	0.0086	0.0030
8.7	2.650	0.033	0.0085	0.0030
8.8	2.651	0.031	0.0083	0.0031
8.9	2.652	0.031	0.0084	0.0035
9	2.652	0.028	0.0084	0.0035
9.1	2.652	0.027	0.0085	0.0033
9.2	2.652	0.028	0.0086	0.0030
9.3	2.652	0.027	0.0086	0.0027
9.4	2.652	0.027	0.0087	0.0026
9.5	2.652	0.028	0.0087	0.0028
9.6	2.652	0.025	0.0088	0.0027
9.7	2.652	0.026	0.0087	0.0031
9.8	2.653	0.027	0.0087	0.0028
9.9	2.654	0.027	0.0088	0.0029
10	2.654	0.028	0.0087	0.0033
10.1	2.655	0.028	0.0086	0.0035
10.2	2.655	0.029	0.0086	0.0039
10.3	2.656	0.030	0.0086	0.0037
10.4	2.656	0.028	0.0086	0.0037
10.5	2.656	0.028	0.0086	0.0035
10.6	2.656	0.033	0.0088	0.0052
10.7	2.653	0.033	0.0092	0.0045
10.8	2.654	0.028	0.0091	0.0031
10.9	2.654	0.028	0.0090	0.0027
11	2.654	0.028	0.0089	0.0025
11.1	2.654	0.030	0.0089	0.0025
11.2	2.656	0.032	0.0088	0.0035
11.3	2.657	0.032	0.0089	0.0034
11.4	2.658	0.034	0.0088	0.0043
11.5	2.658	0.032	0.0089	0.0048
11.6	2.658	0.030	0.0088	0.0052
11.7	2.659	0.033	0.0092	0.0055
11.8	2.657	0.032	0.0090	0.0051
11.9	2.657	0.034	0.0088	0.0045
12	2.657	0.035	0.0087	0.0037

Table 11: Measurement results of the relative permittivity and loss tangent of MAT.TR-KRISS (Acrylic) obtained at NMIJ

Frequency (GHz)	Before sending				After returning			
	ϵ_r	$U(\epsilon_r)$	$\tan \delta$	$U(\tan \delta)$	ϵ_r	$U(\epsilon_r)$	$\tan \delta$	$U(\tan \delta)$
8	2.629	0.022	0.0056	0.0080	2.584	0.021	0.0071	0.0079
8.1	2.631	0.022	0.0060	0.0079	2.587	0.021	0.0073	0.0079
8.2	2.630	0.022	0.0061	0.0078	2.586	0.021	0.0068	0.0079
8.3	2.629	0.022	0.0065	0.0077	2.586	0.021	0.0064	0.0077
8.4	2.629	0.022	0.0061	0.0078	2.586	0.021	0.0063	0.0078
8.5	2.630	0.022	0.0056	0.0079	2.583	0.021	0.0061	0.0078
8.6	2.630	0.022	0.0052	0.0077	2.584	0.021	0.0061	0.0077
8.7	2.629	0.021	0.0058	0.0076	2.583	0.021	0.0060	0.0077
8.8	2.628	0.021	0.0054	0.0079	2.583	0.021	0.0063	0.0076
8.9	2.628	0.021	0.0044	0.0076	2.585	0.021	0.0064	0.0076
9	2.628	0.021	0.0050	0.0076	2.586	0.021	0.0066	0.0074
9.1	2.628	0.021	0.0049	0.0074	2.584	0.021	0.0063	0.0075
9.2	2.627	0.021	0.0049	0.0076	2.584	0.021	0.0056	0.0075
9.3	2.626	0.021	0.0040	0.0075	2.582	0.020	0.0054	0.0075
9.4	2.628	0.021	0.0035	0.0072	2.584	0.020	0.0055	0.0074
9.5	2.627	0.021	0.0036	0.0074	2.583	0.020	0.0060	0.0074
9.6	2.626	0.020	0.0043	0.0072	2.583	0.020	0.0067	0.0073
9.7	2.628	0.020	0.0037	0.0072	2.583	0.020	0.0067	0.0073
9.8	2.629	0.020	0.0038	0.0073	2.584	0.020	0.0071	0.0073
9.9	2.632	0.020	0.0041	0.0072	2.585	0.020	0.0071	0.0072
10	2.630	0.020	0.0048	0.0071	2.585	0.019	0.0068	0.0071
10.1	2.631	0.020	0.0052	0.0071	2.584	0.019	0.0067	0.0072
10.2	2.632	0.020	0.0046	0.0071	2.585	0.019	0.0066	0.0071
10.3	2.633	0.019	0.0050	0.0069	2.584	0.019	0.0062	0.0072
10.4	2.631	0.019	0.0053	0.0069	2.584	0.019	0.0065	0.0070
10.5	2.630	0.019	0.0060	0.0070	2.582	0.019	0.0063	0.0069
10.6	2.630	0.019	0.0055	0.0068	2.584	0.019	0.0065	0.0068
10.7	2.630	0.019	0.0062	0.0069	2.584	0.019	0.0065	0.0066
10.8	2.628	0.019	0.0060	0.0067	2.580	0.019	0.0068	0.0068
10.9	2.628	0.018	0.0064	0.0066	2.580	0.018	0.0060	0.0066
11	2.629	0.018	0.0060	0.0065	2.581	0.018	0.0059	0.0063
11.1	2.627	0.018	0.0059	0.0065	2.581	0.018	0.0056	0.0064
11.2	2.628	0.018	0.0059	0.0064	2.581	0.017	0.0051	0.0064
11.3	2.624	0.018	0.0066	0.0064	2.582	0.017	0.0051	0.0063
11.4	2.622	0.017	0.0075	0.0063	2.582	0.017	0.0051	0.0062
11.5	2.623	0.017	0.0061	0.0061	2.581	0.017	0.0049	0.0062
11.6	2.624	0.017	0.0062	0.0062	2.581	0.017	0.0051	0.0061
11.7	2.625	0.017	0.0058	0.0060	2.580	0.016	0.0053	0.0060
11.8	2.625	0.016	0.0062	0.0061	2.583	0.016	0.0056	0.0060
11.9	2.626	0.016	0.0054	0.0060	2.581	0.016	0.0059	0.0059
12	2.626	0.016	0.0055	0.0059	2.582	0.016	0.0048	0.0058

Table 12: Measurement results of the relative permittivity and loss tangent of MAT.TR-LNE (Acrylic) obtained at NMIJ

Frequency (GHz)	Before sending				After returning			
	ϵ_r	$U(\epsilon_r)$	$\tan \delta$	$U(\tan \delta)$	ϵ_r	$U(\epsilon_r)$	$\tan \delta$	$U(\tan \delta)$
8	2.609	0.022	0.0069	0.0079	2.581	0.022	0.0068	0.0078
8.1	2.610	0.021	0.0073	0.0079	2.583	0.022	0.0069	0.0080
8.2	2.609	0.022	0.0074	0.0078	2.583	0.022	0.0065	0.0078
8.3	2.607	0.021	0.0079	0.0078	2.584	0.022	0.0061	0.0077
8.4	2.606	0.021	0.0074	0.0078	2.583	0.022	0.0059	0.0077
8.5	2.607	0.021	0.0068	0.0077	2.581	0.022	0.0057	0.0077
8.6	2.607	0.021	0.0061	0.0077	2.581	0.022	0.0057	0.0077
8.7	2.607	0.021	0.0066	0.0077	2.580	0.021	0.0057	0.0075
8.8	2.607	0.021	0.0062	0.0077	2.581	0.021	0.0060	0.0077
8.9	2.606	0.021	0.0052	0.0075	2.582	0.021	0.0062	0.0076
9	2.606	0.021	0.0058	0.0075	2.583	0.021	0.0063	0.0075
9.1	2.605	0.021	0.0057	0.0075	2.582	0.021	0.0060	0.0074
9.2	2.604	0.021	0.0057	0.0076	2.582	0.021	0.0053	0.0075
9.3	2.604	0.021	0.0048	0.0074	2.580	0.021	0.0052	0.0075
9.4	2.607	0.020	0.0042	0.0074	2.582	0.021	0.0054	0.0075
9.5	2.606	0.020	0.0044	0.0074	2.581	0.021	0.0058	0.0074
9.6	2.606	0.020	0.0050	0.0073	2.581	0.021	0.0065	0.0075
9.7	2.607	0.020	0.0047	0.0072	2.582	0.021	0.0064	0.0073
9.8	2.607	0.020	0.0049	0.0073	2.582	0.021	0.0069	0.0073
9.9	2.609	0.020	0.0051	0.0072	2.583	0.021	0.0069	0.0073
10	2.608	0.019	0.0057	0.0072	2.583	0.020	0.0066	0.0072
10.1	2.609	0.020	0.0060	0.0072	2.582	0.020	0.0066	0.0071
10.2	2.610	0.019	0.0054	0.0071	2.583	0.020	0.0065	0.0070
10.3	2.610	0.020	0.0057	0.0069	2.582	0.020	0.0062	0.0069
10.4	2.609	0.020	0.0060	0.0068	2.582	0.021	0.0064	0.0070
10.5	2.607	0.019	0.0068	0.0068	2.581	0.020	0.0064	0.0068
10.6	2.607	0.019	0.0063	0.0069	2.581	0.020	0.0065	0.0067
10.7	2.607	0.019	0.0066	0.0067	2.581	0.020	0.0065	0.0067
10.8	2.605	0.019	0.0066	0.0068	2.578	0.019	0.0068	0.0066
10.9	2.605	0.018	0.0070	0.0065	2.579	0.019	0.0062	0.0066
11	2.606	0.019	0.0067	0.0065	2.579	0.019	0.0061	0.0066
11.1	2.605	0.018	0.0064	0.0065	2.579	0.019	0.0058	0.0065
11.2	2.606	0.018	0.0064	0.0064	2.580	0.019	0.0053	0.0064
11.3	2.603	0.018	0.0071	0.0063	2.580	0.019	0.0053	0.0064
11.4	2.601	0.018	0.0079	0.0064	2.580	0.019	0.0052	0.0063
11.5	2.601	0.018	0.0067	0.0062	2.578	0.018	0.0051	0.0063
11.6	2.602	0.017	0.0068	0.0061	2.578	0.018	0.0053	0.0061
11.7	2.603	0.017	0.0063	0.0060	2.578	0.018	0.0054	0.0060
11.8	2.603	0.017	0.0068	0.0059	2.580	0.018	0.0057	0.0060
11.9	2.604	0.016	0.0061	0.0058	2.580	0.018	0.0060	0.0058
12	2.604	0.016	0.0062	0.0057	2.579	0.017	0.0050	0.0058

Table 13: Measurement results of the relative permittivity and loss tangent of MAT.TR-NIM (Acrylic) obtained at NMIJ

Frequency (GHz)	Before sending				After returning			
	ϵ_r	$U(\epsilon_r)$	$\tan \delta$	$U(\tan \delta)$	ϵ_r	$U(\epsilon_r)$	$\tan \delta$	$U(\tan \delta)$
8	2.625	0.022	0.0049	0.0080	2.584	0.022	0.0064	0.0078
8.1	2.626	0.021	0.0052	0.0078	2.587	0.021	0.0065	0.0078
8.2	2.626	0.022	0.0053	0.0077	2.587	0.021	0.0061	0.0077
8.3	2.624	0.022	0.0056	0.0078	2.587	0.021	0.0057	0.0078
8.4	2.625	0.022	0.0051	0.0078	2.587	0.021	0.0056	0.0076
8.5	2.626	0.022	0.0045	0.0078	2.584	0.021	0.0054	0.0078
8.6	2.626	0.022	0.0040	0.0076	2.585	0.021	0.0054	0.0076
8.7	2.626	0.021	0.0046	0.0077	2.584	0.021	0.0053	0.0075
8.8	2.626	0.021	0.0043	0.0076	2.585	0.021	0.0056	0.0074
8.9	2.625	0.022	0.0034	0.0073	2.586	0.021	0.0057	0.0075
9	2.626	0.021	0.0041	0.0077	2.587	0.021	0.0058	0.0074
9.1	2.625	0.021	0.0041	0.0074	2.586	0.021	0.0056	0.0074
9.2	2.625	0.021	0.0043	0.0075	2.586	0.021	0.0048	0.0074
9.3	2.624	0.021	0.0035	0.0072	2.584	0.021	0.0046	0.0073
9.4	2.626	0.021	0.0030	0.0067	2.586	0.020	0.0048	0.0072
9.5	2.625	0.021	0.0033	0.0070	2.585	0.020	0.0052	0.0073
9.6	2.624	0.021	0.0040	0.0074	2.585	0.020	0.0060	0.0073
9.7	2.626	0.020	0.0036	0.0071	2.586	0.020	0.0059	0.0072
9.8	2.626	0.020	0.0038	0.0071	2.586	0.020	0.0065	0.0072
9.9	2.629	0.020	0.0041	0.0072	2.587	0.021	0.0065	0.0071
10	2.627	0.020	0.0047	0.0071	2.588	0.020	0.0062	0.0071
10.1	2.628	0.020	0.0050	0.0071	2.587	0.020	0.0062	0.0070
10.2	2.629	0.020	0.0044	0.0071	2.588	0.020	0.0061	0.0070
10.3	2.629	0.019	0.0048	0.0070	2.586	0.020	0.0057	0.0069
10.4	2.627	0.019	0.0051	0.0069	2.587	0.019	0.0060	0.0068
10.5	2.626	0.019	0.0058	0.0068	2.585	0.019	0.0060	0.0068
10.6	2.626	0.019	0.0053	0.0068	2.586	0.019	0.0061	0.0068
10.7	2.625	0.019	0.0057	0.0067	2.586	0.019	0.0060	0.0067
10.8	2.624	0.019	0.0056	0.0067	2.583	0.019	0.0062	0.0066
10.9	2.624	0.018	0.0059	0.0067	2.583	0.019	0.0056	0.0066
11	2.625	0.018	0.0055	0.0065	2.584	0.019	0.0055	0.0065
11.1	2.623	0.018	0.0054	0.0064	2.584	0.018	0.0053	0.0065
11.2	2.624	0.018	0.0054	0.0064	2.584	0.018	0.0049	0.0064
11.3	2.621	0.018	0.0061	0.0063	2.584	0.018	0.0049	0.0062
11.4	2.619	0.018	0.0070	0.0063	2.584	0.018	0.0048	0.0063
11.5	2.620	0.018	0.0056	0.0061	2.583	0.018	0.0046	0.0062
11.6	2.621	0.018	0.0057	0.0061	2.583	0.017	0.0049	0.0061
11.7	2.622	0.017	0.0053	0.0060	2.583	0.017	0.0050	0.0059
11.8	2.622	0.017	0.0056	0.0059	2.585	0.017	0.0053	0.0059
11.9	2.623	0.017	0.0050	0.0058	2.584	0.017	0.0056	0.0057
12	2.623	0.017	0.0051	0.0057	2.584	0.017	0.0046	0.0057

Table 14: Measurement results of the relative permittivity and loss tangent of MAT.TR-NMC (Acrylic) obtained at NMIJ

Frequency (GHz)	Before sending				After returning			
	ϵ_r	$U(\epsilon_r)$	$\tan \delta$	$U(\tan \delta)$	ϵ_r	$U(\epsilon_r)$	$\tan \delta$	$U(\tan \delta)$
8	2.628	0.022	0.0068	0.0078	2.599	0.022	0.0065	0.0080
8.1	2.629	0.022	0.0071	0.0078	2.601	0.022	0.0067	0.0078
8.2	2.629	0.022	0.0072	0.0079	2.601	0.022	0.0063	0.0078
8.3	2.627	0.022	0.0076	0.0078	2.602	0.022	0.0058	0.0077
8.4	2.627	0.022	0.0071	0.0076	2.601	0.022	0.0056	0.0077
8.5	2.628	0.022	0.0065	0.0078	2.599	0.021	0.0052	0.0077
8.6	2.628	0.022	0.0059	0.0078	2.599	0.022	0.0054	0.0076
8.7	2.628	0.021	0.0063	0.0076	2.598	0.021	0.0054	0.0076
8.8	2.628	0.021	0.0060	0.0076	2.598	0.021	0.0058	0.0077
8.9	2.627	0.021	0.0051	0.0076	2.600	0.021	0.0059	0.0077
9	2.627	0.021	0.0057	0.0077	2.601	0.021	0.0060	0.0076
9.1	2.627	0.021	0.0057	0.0075	2.599	0.021	0.0057	0.0075
9.2	2.626	0.021	0.0057	0.0075	2.600	0.021	0.0050	0.0075
9.3	2.625	0.021	0.0049	0.0076	2.598	0.021	0.0049	0.0074
9.4	2.628	0.021	0.0044	0.0075	2.599	0.021	0.0051	0.0075
9.5	2.627	0.021	0.0046	0.0075	2.599	0.021	0.0055	0.0074
9.6	2.626	0.021	0.0053	0.0074	2.599	0.020	0.0062	0.0073
9.7	2.628	0.020	0.0050	0.0073	2.599	0.021	0.0060	0.0073
9.8	2.627	0.020	0.0052	0.0072	2.600	0.020	0.0064	0.0072
9.9	2.630	0.020	0.0054	0.0072	2.601	0.020	0.0064	0.0072
10	2.629	0.020	0.0060	0.0071	2.601	0.020	0.0062	0.0071
10.1	2.629	0.020	0.0063	0.0071	2.600	0.020	0.0062	0.0070
10.2	2.630	0.020	0.0057	0.0071	2.601	0.020	0.0061	0.0070
10.3	2.631	0.020	0.0059	0.0069	2.599	0.019	0.0057	0.0069
10.4	2.629	0.020	0.0062	0.0070	2.600	0.019	0.0060	0.0070
10.5	2.628	0.019	0.0070	0.0070	2.598	0.020	0.0059	0.0069
10.6	2.627	0.019	0.0067	0.0068	2.599	0.019	0.0061	0.0067
10.7	2.626	0.019	0.0072	0.0072	2.598	0.019	0.0062	0.0068
10.8	2.625	0.019	0.0068	0.0067	2.596	0.019	0.0063	0.0066
10.9	2.625	0.019	0.0072	0.0067	2.597	0.019	0.0059	0.0065
11	2.626	0.018	0.0069	0.0065	2.597	0.018	0.0058	0.0065
11.1	2.624	0.018	0.0066	0.0065	2.597	0.018	0.0054	0.0064
11.2	2.626	0.018	0.0065	0.0064	2.598	0.018	0.0050	0.0064
11.3	2.622	0.018	0.0072	0.0065	2.598	0.018	0.0050	0.0063
11.4	2.620	0.018	0.0081	0.0062	2.598	0.018	0.0050	0.0061
11.5	2.621	0.017	0.0069	0.0062	2.596	0.018	0.0049	0.0061
11.6	2.622	0.017	0.0070	0.0062	2.596	0.017	0.0052	0.0059
11.7	2.623	0.017	0.0065	0.0060	2.596	0.017	0.0055	0.0060
11.8	2.622	0.017	0.0069	0.0060	2.598	0.017	0.0057	0.0060
11.9	2.624	0.017	0.0063	0.0058	2.597	0.017	0.0060	0.0058
12	2.623	0.016	0.0064	0.0059	2.597	0.017	0.0050	0.0057

Table 15: Uncertainty budget of ϵ_r' of MAT.TR-KRISS at 8 GHz

No.	Sources of uncertainty, x_i	$u(x_i)$	$ c_i $	$ c_i u(x_i)$	Probability distribution	Degrees of freedom ⁽³⁾	
1	S-parameters	$ S_{11} $	0.00518	0.02940	0.00015	Rect.	∞
		$ S_{12} $	0.00303	0.00579	0.00002	Rect.	∞
		$ S_{21} $	0.00303	0.00579	0.00002	Rect.	∞
		$ S_{22} $	0.00518	0.02940	0.00015	Rect.	∞
		θ_{11}	0.00901	0.85353	0.00769	Rect.	∞
		θ_{12}	0.00557	0.96852	0.00539	Rect.	∞
		θ_{21}	0.00557	0.96852	0.00539	Rect.	∞
		θ_{22}	0.00901	0.85353	0.00769	Rect.	∞
	Combined uncertainty			0.01328	Normal	∞	
2	Thickness of the fixture	0.84e-3 (mm)	424.39 (1/m)	0.00036	t – dist	17	
3	Thickness of the sample	1.1e-3 (mm)	424.39 (1/m)	0.00047	t – dist	10	
4	Width of fixture aperture (22.86 mm)	0.84 ⁽²⁾ (mm)	- ⁽¹⁾	0.00084	Rect.	∞	
5	Height of fixture aperture (10.16 mm)	7.0e-7 ⁽²⁾ (mm)	- ⁽¹⁾	7.0e-10	Rect.	∞	
6	Repeatability			0.00118	t – dist	5	
	Combined standard uncertainty ($k = 1$)			0.01337	Normal	1.2e+4	

(1) Calculated by Monte Carlo simulation (Number of simulation = 10,000)

(2) Tolerance given by manufacturer. A rectangular distribution is assumed.

(3) To calculate effective degrees of freedom ∞ is set as 1e+10.

Table 16: Uncertainty budget of ϵ_r' of MAT.TR-KRISS at 10 GHz

No.	Sources of uncertainty x_i	$u(x_i)$	$ c_i $	$ c_i u(x_i)$	Probability distribution	Degrees of freedom ⁽³⁾	
1	S-parameters	$ S_{11} $	0.00508	0.02126	0.00011	Rect.	1
		$ S_{12} $	0.00307	0.00634	0.00002	Rect.	∞
		$ S_{21} $	0.00307	0.00634	0.00002	Rect.	∞
		$ S_{22} $	0.00508	0.02124	0.00011	Rect.	∞
		θ_{11}	0.01032	0.61154	0.00631	Rect.	∞
		θ_{12}	0.00552	1.14400	0.00631	Rect.	∞
		θ_{21}	0.00552	1.14400	0.00631	Rect.	∞
		θ_{22}	0.01032	0.61154	0.00631	Rect.	∞
	Combined uncertainty			0.01263	Normal	∞	
2	Thickness of the fixture	0.84e-3 (mm)	909.44 (1/m)	0.00076	t – dist	17	
3	Thickness of the sample	1.1e-3 (mm)	909.44 (1/m)	0.00100	t – dist	10	
4	Width of fixture aperture (22.86 mm)	0.72 ⁽²⁾ (mm)	- ⁽¹⁾	0.00072	Rect.	∞	
5	Height of fixture aperture (10.16 mm)	6.0e-7 ⁽²⁾ (mm)	- ⁽¹⁾	6.0e-10	Rect.	∞	
6	Repeatability	-	-	0.00124	t – dist	5	
	Combined standard uncertainty ($k = 1$)			0.01277	Normal	7.7e+3	

(1) Calculated by Monte Carlo simulation (Number of simulation = 10,000)

(2) Tolerance given by manufacturer. A rectangular distribution is assumed.

(3) To calculate effective degrees of freedom ∞ is set as 1e+10.

Table 17: Uncertainty budget of ϵ_r' of MAT.TR-KRISS at 12 GHz

No.	Sources of uncertainty x_i	$u(x_i)$	$ c_i $	$ c_i u(x_i)$	Probability distribution	Degrees of freedom ⁽³⁾	
1	S-parameters	$ S_{11} $	0.00496	0.01113	0.00006	Rect.	1
		$ S_{12} $	0.00315	0.00507	0.00002	Rect.	∞
		$ S_{21} $	0.00315	0.00507	0.00002	Rect.	∞
		$ S_{22} $	0.00496	0.01112	0.00006	Rect.	∞
		θ_{11}	0.01183	0.41388	0.00489	Rect.	∞
		θ_{12}	0.00575	1.13380	0.00652	Rect.	∞
		θ_{21}	0.00575	1.13380	0.00652	Rect.	∞
		θ_{22}	0.01183	0.41388	0.00489	Rect.	∞
	Combined uncertainty				0.01154	Normal	∞
2	Thickness of the fixture	0.84e-3 (mm)	1246.6 (1/m)	0.00105	t – dist	17	
3	Thickness of the sample	1.1e-3 (mm)	1246.6 (1/m)	0.00137	t – dist	10	
4	Width of fixture aperture (22.86 mm)	0.54 ⁽²⁾ (mm)	- ⁽¹⁾	0.00054	Rect.	∞	
5	Height of fixture aperture (10.16 mm)	4.5e-7 ⁽²⁾ (mm)	- ⁽¹⁾	4.5e-10	Rect.	∞	
6	Repeatability	-	-	0.00127	t – dist	5	
Combined standard uncertainty ($k = 1$)				0.01174	Normal	4.8e+3	

(1) Calculated by Monte Carlo simulation (Number of simulation = 10,000)

(2) Tolerance given by manufacturer. A rectangular distribution is assumed.

(3) To calculate effective degrees of freedom ∞ is set as 1e+10.

Table 18: Uncertainty budget of ϵ_r'' of MAT.TR-KRISS at 8 GHz

No.	Sources of uncertainty x_i	$u(x_i)$	$ c_i $	$ c_i u(x_i)$	Probability distribution	Degrees of freedom ⁽³⁾	
1	S-parameters	$ S_{11} $	0.00518	1.25430	0.00649	Rect.	1
		$ S_{12} $	0.00303	1.33630	0.00404	Rect.	∞
		$ S_{21} $	0.00303	1.33630	0.00405	Rect.	∞
		$ S_{22} $	0.00518	1.25430	0.00649	Rect.	∞
		θ_{11}	0.00901	0.02001	0.00018	Rect.	∞
		θ_{12}	0.00557	0.00419	0.00002	Rect.	∞
		θ_{21}	0.00557	0.00419	0.00002	Rect.	∞
		θ_{22}	0.00901	0.02001	0.00018	Rect.	∞
	Combined uncertainty				0.01082	Normal	∞
2	Thickness of the fixture	0.84e-3 (mm)	340.93 (1/m)	0.00029	t – dist	17	
3	Thickness of the sample	1.1e-3 (mm)	340.93 (1/m)	0.00038	t – dist	10	
4	Width of fixture aperture (22.86 mm)	0.01 ⁽²⁾ (mm)	- ⁽¹⁾	0.00001	Rect.	∞	
5	Height of fixture aperture (10.16 mm)	1.0e-8 ⁽²⁾ (mm)	- ⁽¹⁾	1.0e-11	Rect.	∞	
6	Repeatability	-	-	0.00013	t – dist	5	
Combined standard uncertainty ($k = 1$)				0.01083	Normal	1.8e+6	

(1) Calculated by Monte Carlo simulation (Number of simulation = 10,000)

(2) Tolerance given by manufacturer. A rectangular distribution is assumed.

(3) To calculate effective degrees of freedom ∞ is set as 1e+10.

Table 19: Uncertainty budget of ϵ_r'' of MAT.TR-KRISS at 10 GHz

No.	Sources of uncertainty x_i	$u(x_i)$	$ c_i $	$ c_i u(x_i)$	Probability distribution	Degrees of freedom ⁽³⁾	
1	S-parameters	$ S_{11} $	0.00508	1.04280	0.00530	Rect.	1
		$ S_{12} $	0.00307	1.42600	0.00437	Rect.	∞
		$ S_{21} $	0.00307	1.42590	0.00437	Rect.	∞
		$ S_{22} $	0.00508	1.04210	0.00530	Rect.	∞
		θ_{11}	0.01032	0.01247	0.00013	Rect.	∞
		θ_{12}	0.00552	0.00508	0.00003	Rect.	∞
		θ_{21}	0.00552	0.00508	0.00003	Rect.	∞
		θ_{22}	0.01032	0.01247	0.00013	Rect.	∞
	Combined uncertainty				0.00972	Normal	∞
2	Thickness of the fixture	0.84e-3 (mm)	423.81 (1/m)	0.00036	t – dist	17	
3	Thickness of the sample	1.1e-3 (mm)	423.81 (1/m)	0.00047	t – dist	10	
4	Width of fixture aperture (22.86 mm)	0.01 ⁽²⁾ (mm)	- ⁽¹⁾	0.00001	Rect.	∞	
5	Height of fixture aperture (10.16 mm)	6.4e-9 ⁽²⁾ (mm)	- ⁽¹⁾	6.4e-12	Rect.	∞	
6	Repeatability	-	-	0.00012	t – dist	5	
Combined standard uncertainty ($k = 1$)				0.00974	Normal	7.7e+5	

(1) Calculated by Monte Carlo simulation (Number of simulation = 10,000)

(2) Tolerance given by manufacturer. A rectangular distribution is assumed.

(3) To calculate effective degrees of freedom ∞ is set as 1e+10.

Table 20: Uncertainty budget of ϵ_r'' of MAT.TR-KRISS at 12 GHz

No.	Sources of uncertainty x_i	$u(x_i)$	$ c_i $	$ c_i u(x_i)$	Probability distribution	Degrees of freedom ⁽³⁾	
1	S-parameters	$ S_{11} $	0.00496	0.80632	0.00400	Rect.	1
		$ S_{12} $	0.00315	1.33400	0.00420	Rect.	∞
		$ S_{21} $	0.00315	1.33400	0.00420	Rect.	∞
		$ S_{22} $	0.00496	0.80558	0.00399	Rect.	∞
		θ_{11}	0.01183	0.00571	0.00007	Rect.	∞
		θ_{12}	0.00575	0.00431	0.00002	Rect.	∞
		θ_{21}	0.00575	0.00431	0.00002	Rect.	∞
		θ_{22}	0.01183	0.00571	0.00007	Rect.	∞
	Combined uncertainty				0.00820	Normal	∞
2	Thickness of the fixture	0.84e-3 (mm)	251.16 (1/m)	0.00021	t – dist	17	
3	Thickness of the sample	1.1e-3 (mm)	251.16 (1/m)	0.00028	t – dist	10	
4	Width of fixture aperture (22.86 mm)	4.18e-3 ⁽²⁾ (mm)	- ⁽¹⁾	4.18e-6	Rect.	∞	
5	Height of fixture aperture (10.16 mm)	3.54e-9 ⁽²⁾ (mm)	- ⁽¹⁾	3.54e-12	Rect.	∞	
6	Repeatability	-	-	0.00011	t – dist	5	
Combined standard uncertainty ($k = 1$)				0.00821	Normal	6.0e+5	

(1) Calculated by Monte Carlo simulation (Number of simulation = 10,000)

(2) Tolerance given by manufacturer. A rectangular distribution is assumed.

(3) To calculate effective degrees of freedom ∞ is set as 1e+10.

Table 21: Uncertainty budget of $\tan \delta$ of MAT.TR-KRISS at 8 GHz

No.	Sources of uncertainty x_i	$u(x_i)$	$ c_i $	$ c_i u(x_i)$	Probability distribution	Degrees of freedom
1	ϵ_r'	0.01337	0.00307	0.00004	Normal	2.6e+6
2	ϵ_r''	0.01083	0.37804	0.00409	Normal	2.5e+6
Combined standard uncertainty ($k = 1$)				0.00409	Normal	2.5e+6

Table 22: Uncertainty budget of $\tan \delta$ of MAT.TR-KRISS at 10 GHz

No.	Sources of uncertainty x_i	$u(x_i)$	$ c_i $	$ c_i u(x_i)$	Probability distribution	Degrees of freedom
1	ϵ_r'	0.01277	0.00308	0.00004	Normal	2.1e+6
2	ϵ_r''	0.00974	0.37843	0.00369	Normal	1.6e+6
Combined standard uncertainty ($k = 1$)				0.00369	Normal	1.6e+6

Table 23: Uncertainty budget of $\tan \delta$ of MAT.TR-KRISS at 12 GHz

No.	Sources of uncertainty x_i	$u(x_i)$	$ c_i $	$ c_i u(x_i)$	Probability distribution	Degrees of freedom
1	ϵ_r'	0.01174	0.00311	0.00004	Normal	1.4e+5
2	ϵ_r''	0.00821	0.37871	0.00311	Normal	6.4e+5
Combined standard uncertainty ($k = 1$)				0.00311	Normal	6.4e+5

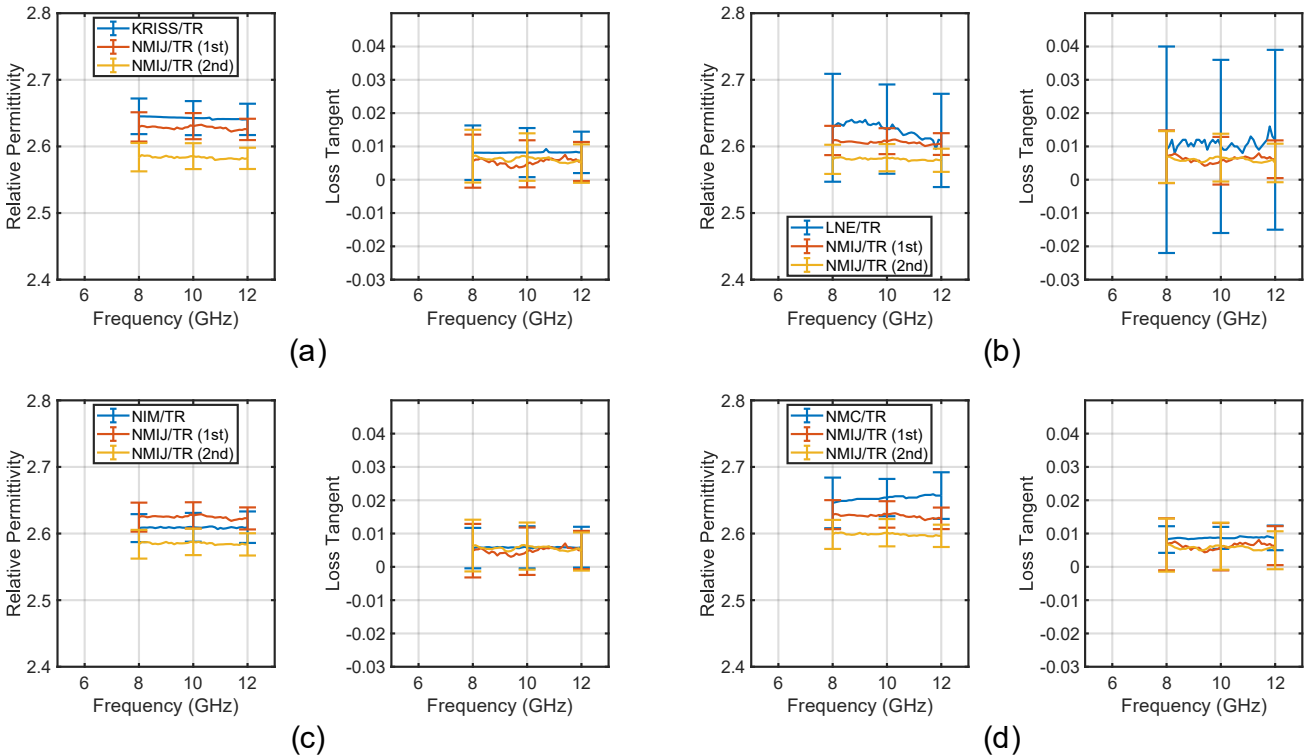


Fig. 6 Measurement results of the relative permittivity and loss tangent of the acrylic samples. (a) MAT.TR-KRISS. (b) MAT.TR-LNE. (c) MAT.TR-NIM. (d) MAT.TR-NMC.

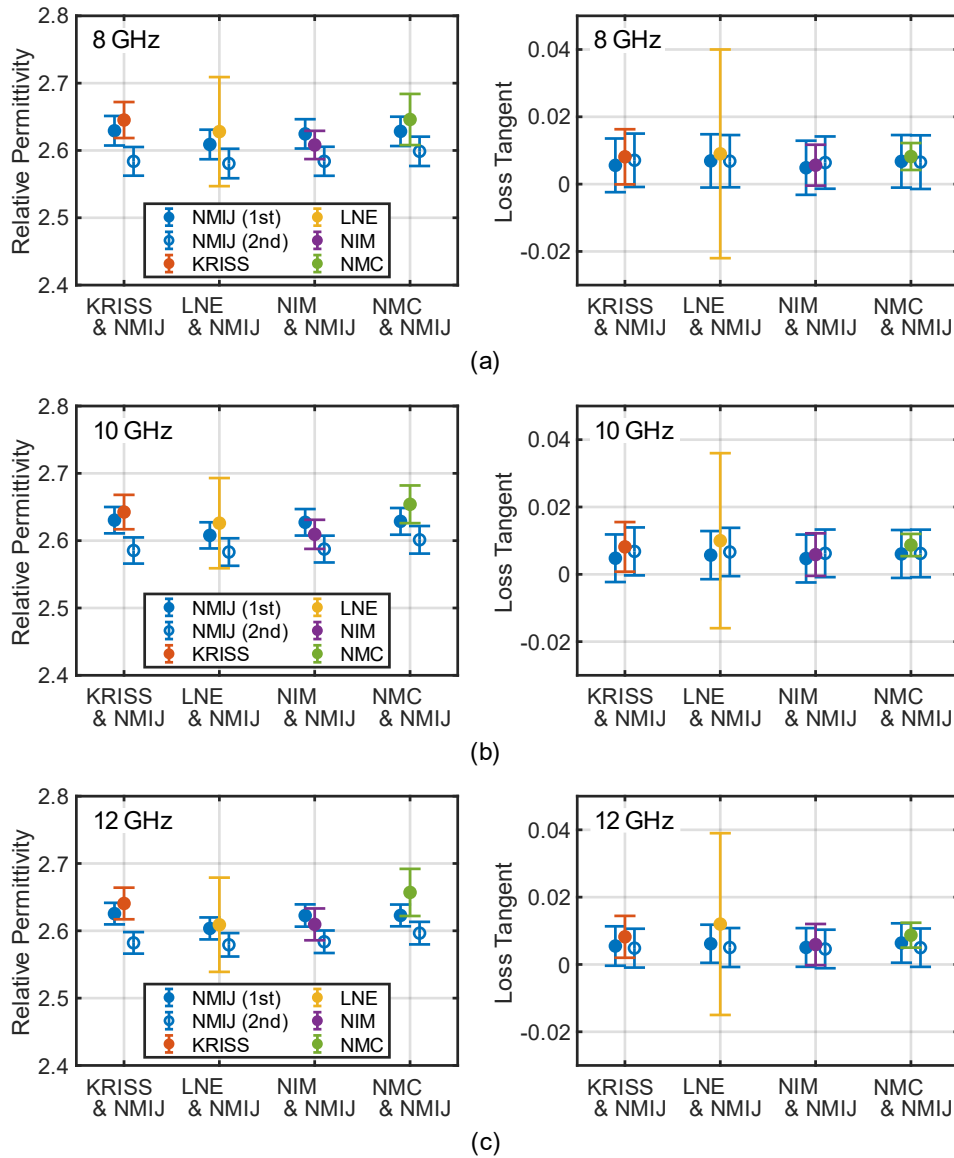


Fig. 7 Measurement results and uncertainties for the relative permittivity and loss tangent of the acrylic samples. (a) At 8 GHz. (b) At 10 GHz. (c) At 12 GHz.

5.4 Discussions

It is seen from Figs. 6 and 7 that the measurement results of the relative permittivity obtained at NMIJ after returning the samples are lower than those before sending the samples. The average reductions over all frequency points are 0.045, 0.025, 0.040, and 0.028 for MAT.TR-KRISS, MAT.TR-LNE, MAT.TR-NIM, and MAT.TR-NMC, respectively. The reason for the reductions is not clear; however, the physical properties of the acrylic samples would have changed during transportation and measurements over several years. The lesson from this is that the pilot laboratory should have a spare sample and measure it periodically to assess the long-term stability of the sample. In contrast, regarding the loss tangent, the measurement results obtained at NMIJ before and after the sample transportation are almost the same within the uncertainties.

Considering the uncertainty of each laboratory and the change in the sample properties during the comparison, the relative permittivity results of the participating laboratories and those of NMIJ are in

good agreement. The loss tangent results are consistent within the uncertainties. While this result would support the equivalence of the loss tangent measurements of the participating laboratories, it is also attributed to the fact that the loss tangent uncertainties are comparable to or larger than the measured values.

For each sample of MAT-TR-XXX (XXX = KRISS, LNE, NIM, and NMC), the DoEs between the following three results and their uncertainties were calculated at 8 GHz, 10 GHz, and 12 GHz for the relative permittivity and loss tangent as shown in Tables 24—31:

- (i) Results obtained at XXX
- (ii) Results obtained at NMIJ before sending the samples (NMIJ/1st)
- (iii) Results obtained at NMIJ after returning the samples (NMIJ/2nd)

Here, DoE and its uncertainty between the measurement results m_x and m_y are defined by: $\text{DoE} = |m_x - m_y|$ and $U(\text{DoE}) = \sqrt{U(m_x)^2 + U(m_y)^2}$, respectively, where $U(m_x)$ and $U(m_y)$ are the uncertainties of m_x and m_y , respectively.

Table 24: Degrees of equivalence and their uncertainties for the relative permittivity results of MAT.TR-KRISS

Frequency (GHz)	KRISS vs NMIJ/1st		KRISS vs NMIJ/2nd		NMIJ/1st vs NMIJ/2nd	
	DoE	$U(\text{DoE})$	DoE	$U(\text{DoE})$	DoE	$U(\text{DoE})$
8	0.016	0.035	0.061	0.034	0.045	0.031
10	0.012	0.032	0.057	0.032	0.045	0.028
12	0.015	0.028	0.058	0.028	0.043	0.023

Table 25: Degrees of equivalence and their uncertainties for the loss tangent results of MAT.TR-KRISS

Frequency (GHz)	KRISS vs NMIJ/1st		KRISS vs NMIJ/2nd		NMIJ/1st vs NMIJ/2nd	
	DoE	$U(\text{DoE})$	DoE	$U(\text{DoE})$	DoE	$U(\text{DoE})$
8	0.0025	0.0114	0.0010	0.0114	0.0015	0.0112
10	0.0034	0.0102	0.0013	0.0103	0.0020	0.0100
12	0.0027	0.0085	0.0034	0.0085	0.0006	0.0082

Table 26: Degrees of equivalence and their uncertainties for the relative permittivity results of MAT.TR-LNE

Frequency (GHz)	LNE vs NMIJ/1st		LNE vs NMIJ/2nd		NMIJ/1st vs NMIJ/2nd	
	DoE	$U(\text{DoE})$	DoE	$U(\text{DoE})$	DoE	$U(\text{DoE})$
8	0.019	0.084	0.047	0.084	0.028	0.031
10	0.018	0.070	0.043	0.070	0.025	0.028
12	0.005	0.072	0.030	0.072	0.024	0.024

Table 27: Degrees of equivalence and their uncertainties for the loss tangent results of MAT.TR-LNE

Frequency (GHz)	LNE vs NMIJ/1st		LNE vs NMIJ/2nd		NMIJ/1st vs NMIJ/2nd	
	DoE	$U(\text{DoE})$	DoE	$U(\text{DoE})$	DoE	$U(\text{DoE})$
8	0.0021	0.0320	0.0022	0.0320	0.0001	0.0111
10	0.0043	0.0270	0.0034	0.0270	0.0009	0.0101
12	0.0058	0.0276	0.0070	0.0276	0.0011	0.0081

Table 28: Degrees of equivalence and their uncertainties for the relative permittivity results of MAT.TR-NIM

Frequency (GHz)	NIM vs NMIJ/1st		NIM vs NMIJ/2nd		NMIJ/1st vs NMIJ/2nd	
	DoE	$U(\text{DoE})$	DoE	$U(\text{DoE})$	DoE	$U(\text{DoE})$
8	0.016	0.030	0.024	0.030	0.041	0.031
10	0.018	0.029	0.022	0.029	0.040	0.028
12	0.013	0.029	0.026	0.029	0.039	0.024

Table 29: Degrees of equivalence and their uncertainties for the loss tangent results of MAT.TR-NIM

Frequency (GHz)	NIM vs NMIJ/1st		NIM vs NMIJ/2nd		NMIJ/1st vs NMIJ/2nd	
	DoE	$U(\text{DoE})$	DoE	$U(\text{DoE})$	DoE	$U(\text{DoE})$
8	0.0008	0.0101	0.0008	0.0099	0.0015	0.0112
10	0.0012	0.0095	0.0004	0.0095	0.0015	0.0100
12	0.0009	0.0084	0.0013	0.0084	0.0004	0.0081

Table 30: Degrees of equivalence and their uncertainties for the relative permittivity results of MAT.TR-NMC

Frequency (GHz)	NMC vs NMIJ/1st		NMC vs NMIJ/2nd		NMIJ/1st vs NMIJ/2nd	
	DoE	$U(\text{DoE})$	DoE	$U(\text{DoE})$	DoE	$U(\text{DoE})$
8	0.018	0.044	0.047	0.044	0.030	0.031
10	0.025	0.034	0.053	0.035	0.027	0.029
12	0.034	0.039	0.060	0.039	0.026	0.023

Table 31: Degrees of equivalence and their uncertainties for the loss tangent results of MAT.TR-NMC

Frequency (GHz)	NMC vs NMIJ/1st		NMC vs NMIJ/2nd		NMIJ/1st vs NMIJ/2nd	
	DoE	$U(\text{DoE})$	DoE	$U(\text{DoE})$	DoE	$U(\text{DoE})$
8	0.0014	0.0088	0.0017	0.0089	0.0002	0.0112
10	0.0027	0.0078	0.0025	0.0078	0.0002	0.0100
12	0.0023	0.0069	0.0037	0.0068	0.0014	0.0082

Regarding the relative permittivity results, the DoE between (i) and (ii) is larger than or comparable to the corresponding $U(\text{DoE})$ for all the samples and frequencies. This indicates that non-negligible property changes occurred in the samples. At least one of the DoEs between (i) and (ii) or (i) and (iii) is less than the corresponding $U(\text{DoE})$ for all the samples and frequencies. This indicates that the relative permittivity

results of KRISS, LNE, NIM, and NMC are consistent with those of NMIJ considering the change in the sample properties during the comparison. Regarding the loss tangent results, the DoEs between (i) and (ii), (i) and (iii), and (ii) and (iii) is less than the corresponding $U(\text{DoE})$ for all the samples and frequencies. This supports that the loss tangent measurements of each participating laboratory were consistent with each other, and that the loss tangent of the samples did not change significantly during the comparison.

6 Resonator method

6.1 Comparison protocol

Three samples were prepared for material characterization based on resonator methods (MAT.RES1-XXX, MAT.RES2-XXX, and MAT.RES3-XXX). Each sample was measured at least at one frequency point within 20—60 GHz. The measurement method and frequencies differ among participating laboratories. All three participating laboratories used the split cylinder resonator (SCR) method, and NMIJ additionally used the balanced-type circular disk resonator (BCDR) method. The details of the measurement systems of the participating laboratories are described in Section 6.2. The general information on the SCR and BCDR methods is described as follows.

(1) SCR method [4,7]

Figure 8(a) shows the schematic of an SCR. It consists of two coaxial cylindrical cavities with a dielectric sheet sample to be measured sandwiched between the cavities. Coupling loops are commonly used to excite and detect electromagnetic modes in the SCR, which are inserted into the resonator through excitation holes on walls of the cavities. The complex permittivity measurements using the SCR method are basically based on the TE_{011} mode resonance, but higher-order modes can also be utilized. When the TE modes are used, the in-plane complex permittivity of the sheet sample is measured.

(2) BCDR method [8-11]

Figure 8(b) shows the schematic of a BCDR. It consists of a thin copper conductor disk sandwiched between a pair of dielectric sheet samples to be measured. The dielectric sheets and conductor disk are sandwiched between two parallel copper plates. The resonator is excited and detected by coaxial lines through excitation holes located at the center of the resonator. In the BCDR, only the TM_{0m0} modes are selectively excited due to the cylindrical symmetry of the resonator. This broadband mode-selective behavior allows broadband material measurements at microwave and millimeter-wave bands by utilizing higher-order TM_{0m0} mode resonances. The complex permittivity normal to the sheet sample is measured at each resonant frequency of the TM_{0m0} modes.

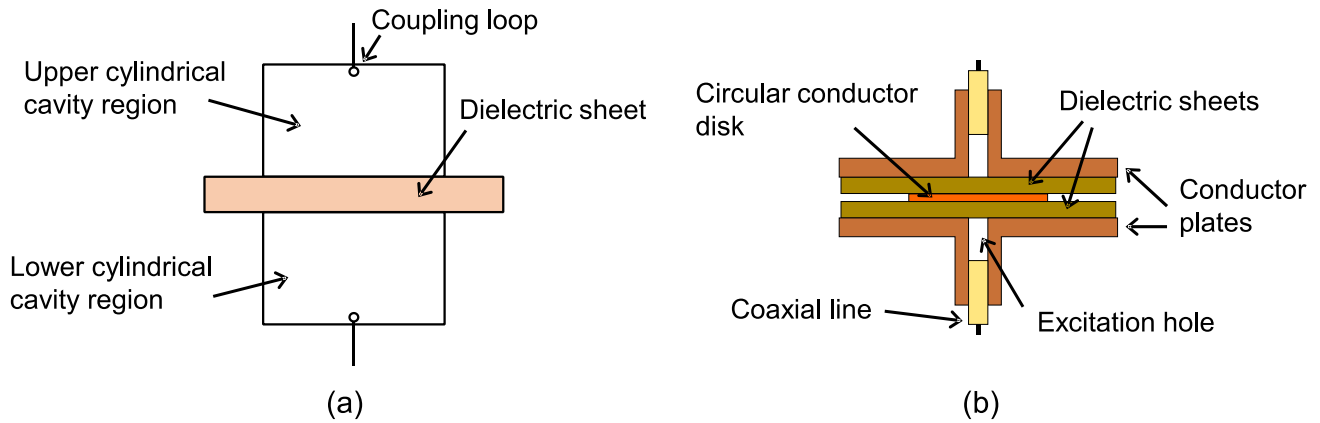


Fig. 8 Schematics of (a) SCR and (b) BCDR

6.2 Measurement systems of participating laboratories

(1) KRISS

SCR method using 85072A from Keysight Technologies was used with a VNA to measure the resonant frequencies and Q-factors at TE_{011} base resonant mode (around 10 GHz) without a sample and at a higher order mode near 28 GHz with a sample. A micrometer was used to measure the sample thicknesses. The dimensions of the resonator were not measured and those from the manufacturer were used instead. The sample size required by 85072A, a 10-GHz SCR, is a minimum length or diameter of 56 mm, but the length of the traveling samples is 40 or 50 mm, which is not satisfied with the length requirement of the SCR. This may affect the measured value.

For KRISS, relative permittivity measurements are traceable, via the traceability of impedance and attenuation measurements and length measurements, to the SI.

The measurement conditions were as follows:

- Temperature: $(23.0 \pm 0.5) ^\circ\text{C}$
- Relative humidity: $(50 \pm 10) \%$

(2) NIM

A SCR was developed to measure the complex permittivity of the COP sheet, as shown in Fig. 9. The AQ and EN-AI samples were seriously damaged when NIM got the package. The resonant frequency of the TE_{011} mode was approximately 10 GHz with no sample and no gap between the two cylindrical-cavity sections. The relative permittivity and loss tangent were calculated from the resonant frequencies, Q-factors and the dimensions of the sample and resonator by using the mode-matching method. NIM employed the higher-order resonance modes to obtain the relative permittivity and loss tangent at frequencies higher than 20 GHz. The uncertainties of the resonant frequency, Q-factor, dimensions of the sample and resonator and the error of the mode-matching analysis were considered to calculate the total measurement uncertainty.

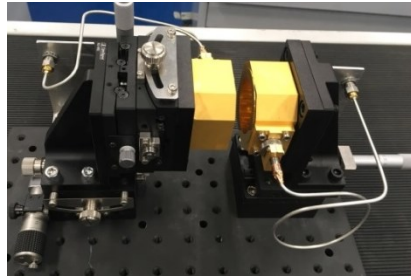


Fig. 9 The 10 GHz SCR developed at NIM

(3) NMIJ

Figure 10(a) shows the SCR developed at NMIJ. The resonant frequency of the TE_{011} mode without a sample was approximately 24 GHz. The dimensions and conductivity of the resonator were calculated from the measured resonant frequencies and Q-factors of the TE_{011} and TM_{011} modes of the SCR without a sample. The relative permittivity and loss tangent of the sheet samples were calculated from the measured resonant frequencies and Q-factors of the TE_{011} mode of the SCR after loading each sheet sample by using the mode-matching analysis. The measurement results of the dimensions of the sample and resonator and the conductivity of the resonator were also used in calculating the sample complex permittivity. The uncertainties of all measurands (resonant frequency, Q-factor, dimensions, and conductivity), as well as the error of the mode-matching analysis, were considered to calculate the total measurement uncertainty of the relative permittivity and loss tangent [7].

Figure 10(b) shows the BCDR developed at NMIJ. The resonator is excited and detected by 1 mm coaxial lines. A copper disk with a diameter of approximately 15 mm and a thickness of approximately 0.06 mm was used. The relative permittivity and loss tangent of the sheet samples were calculated from the measured resonant frequencies and Q-factors of the TM_{0m0} modes of the BCDR by using the mode-matching analysis. The dimensions of the sample and copper disk were also used in the analysis. The conductivity of the copper measured at 10 GHz by using the two-dielectric resonator method was also used in calculating the sample complex permittivity. The uncertainties of all measurands (resonant frequency, Q-factor, dimensions, and conductivity), as well as the error of the mode-matching analysis, were considered to calculate the total measurement uncertainty of the relative permittivity and loss tangent [10,11].

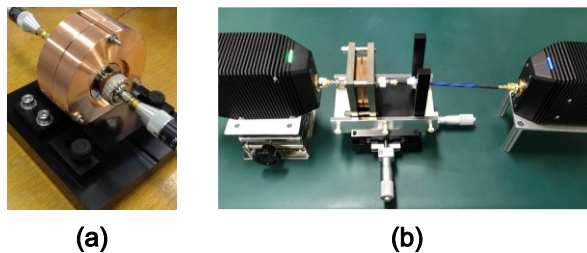


Fig. 10 (a) SCR and (b) BCDR used at NMIJ for the comparison

6.3 Results

(1) MAT-RES-KRISS

The measurement results for MAT-RES1-KRISS, MAT-RES2-KRISS, and MAT-RES3-KRISS are shown in Tables 32—34 and Fig. 11(a)—(c). In the tables, the measurement method and the direction of the measured permittivity are also presented. Measurement uncertainties in the tables and figures are the

expanded values with a coverage factor $k = 2$. For the measurements at KRISS, the measurement uncertainties were not estimated because the sample size did not meet the minimum size requirement of the 85072A used for the comparison. For the information, the standard deviations from repeated measurements are shown in Table 35.

Table 32: Measurement results of the relative permittivity and loss tangent of MAT.RES1-KRISS (COP)

Laboratory	Frequency (GHz)	ϵ_r	$U(\epsilon_r)$	$\tan \delta$	$U(\tan \delta)$	Method	Direction
KRISS	26.77201	2.3442	—	0.00057	—	SCR	In-plane
NMIJ (measurements before sending the samples to KRISS)	23.18110	2.3178	0.0093	0.00034	0.00004	SCR	In-plane
	15.83953	2.3301	0.0082	0.00029	0.00021	BCDR	Perpendicular
	29.19144	2.3274	0.0121	0.00035	0.00006		
	42.54039	2.3264	0.0150	0.00036	0.00003		
	55.92096	2.3258	0.0168	0.00039	0.00004		
69.31244	2.3257	0.0180	0.00038	0.00004			
NMIJ (measurements after returning the samples from KRISS)	23.18010	2.3200	0.0093	0.00035	0.00004	SCR	In-plane
	15.83953	2.3301	0.0082	0.00029	0.00021	BCDR	Perpendicular
	29.19144	2.3274	0.0121	0.00035	0.00006		
	42.54039	2.3264	0.0150	0.00036	0.00003		
	55.92096	2.3258	0.0168	0.00039	0.00004		
69.31244	2.3257	0.0180	0.00038	0.00004			

Table 33: Measurement results of the relative permittivity and loss tangent of MAT.RES2-KRISS (Silica glass)

Laboratory	Frequency (GHz)	ϵ_r	$U(\epsilon_r)$	$\tan \delta$	$U(\tan \delta)$	Method	Direction
KRISS	26.56529	3.8144	—	0.00021	—	SCR	In-plane
NMIJ (measurements before sending the samples to KRISS)	22.29691	3.7910	0.0222	0.00010	0.00002	SCR	In-plane
	12.45569	3.7526	0.0140	0.00007	0.00011	BCDR	Perpendicular
	22.95579	3.7495	0.0209	0.00011	0.00010		
	33.45474	3.7485	0.0260	0.00014	0.00004		
	43.97936	3.7478	0.0295	0.00018	0.00004		
	54.51422	3.7477	0.0319	0.00023	0.00006		
65.03937	3.7481	0.0335	0.00028	0.00004			
NMIJ (measurements after returning the samples from KRISS)	22.29583	3.7930	0.0222	0.00010	0.00002	SCR	In-plane
	12.45569	3.7526	0.0140	0.00007	0.00011	BCDR	Perpendicular
	22.95579	3.7495	0.0209	0.00011	0.00010		
	33.45474	3.7485	0.0260	0.00014	0.00004		
	43.97936	3.7478	0.0295	0.00018	0.00004		
	54.51422	3.7477	0.0319	0.00023	0.00006		
65.03937	3.7481	0.0335	0.00028	0.00004			

Table 34: Measurement results of the relative permittivity and loss tangent of MAT.RES3-KRISS (Alkali-free glass)

Laboratory	Frequency (GHz)	ϵ_r	$U(\epsilon_r)$	$\tan \delta$	$U(\tan \delta)$	Method	Direction
KRISS	26.41716	5.4859	—	0.00753	—	SCR	In-plane
NMIJ (measurements before sending the samples to KRISS)	21.28023	5.4883	0.0178	0.00691	0.00025	SCR	In-plane
	10.39676	5.3784	0.0230	0.00584	0.00029	BCDR	Perpendicular
	19.18624	5.3619	0.0334	0.00690	0.00014		
	27.97573	5.3563	0.0442	0.00755	0.00025		
	36.80359	5.3484	0.0472	0.00811	0.00029		
	45.66324	5.3385	0.0514	0.00866	0.00048		
	54.48091	5.3391	0.0567	0.00946	0.00037		
63.32617	5.3311	0.0598	0.00965	0.00042			
NMIJ (measurements after returning the samples from KRISS)	21.27841	5.4917	0.0190	0.00711	0.00051	SCR	In-plane
	10.39676	5.3784	0.0230	0.00584	0.00029	BCDR	Perpendicular
	19.18624	5.3619	0.0334	0.00690	0.00014		
	27.97573	5.3563	0.0442	0.00755	0.00025		
	36.80359	5.3484	0.0472	0.00811	0.00029		
	45.66324	5.3385	0.0514	0.00866	0.00048		
	54.48091	5.3391	0.0567	0.00946	0.00037		
	63.32617	5.3311	0.0598	0.00965	0.00042		

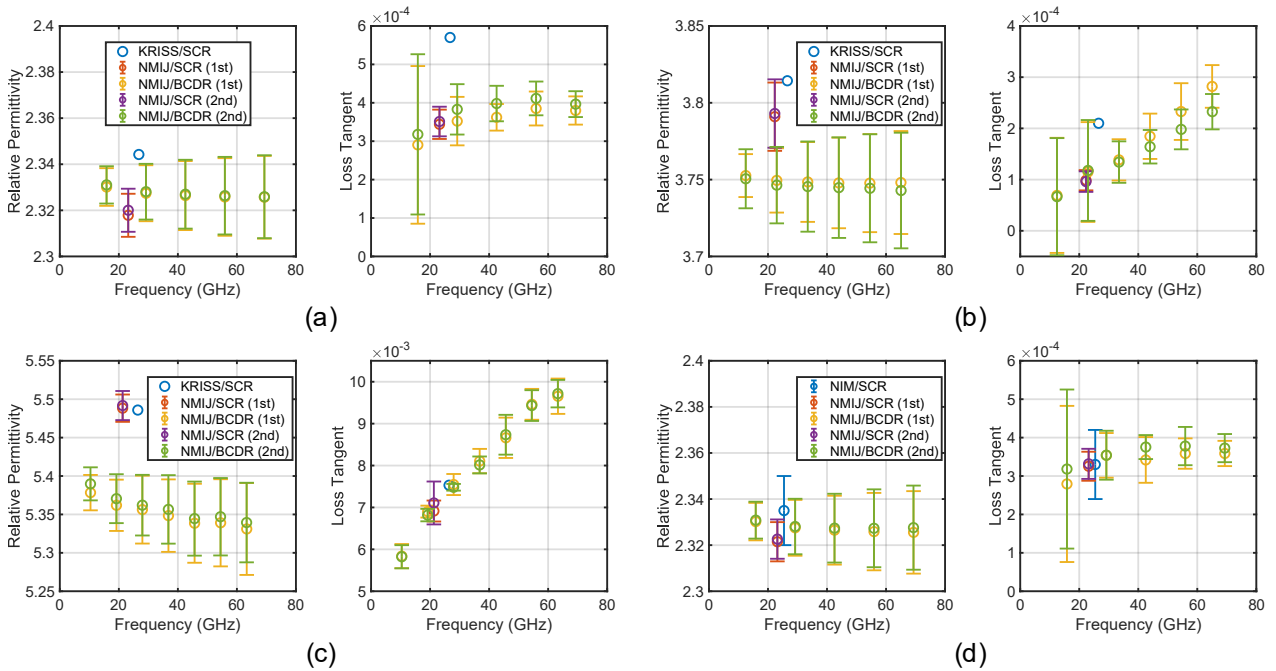


Fig. 11 Measurement results of the relative permittivity and loss tangent of the resonator samples. (a) MAT.RES1-KRISS (COP). (b) MAT.RES2-KRISS (Silica glass). (c) MAT.RES3-KRISS (Alkali-free glass). (d) MAT.RES1-NIM (COP).

Table 35. Standard deviations of the measurements at KRISS

Sample	MAT.RES1-KRISS (COP)	MAT.RES2-KRISS (Silica glass)	MAT.RES3-KRISS (Alkali-free glass)
Resonant freq. (MHz)	0.06203	0.23191	0.07689
$u(\epsilon_r')$ ($\times 10^3$)	0.807	1.128	1.677
$u(\tan \delta)$ ($\times 10^5$)	5.6	2.3	4.2
# of measurements	10	14	11

(2) MAT-RES-NIM

The measurement results for MAT-RES1-NIM are shown in Table 36 and Fig. 11(d). In the table, the measurement method and the direction of the measured permittivity are also presented. Measurement uncertainties in the table and figure are the expanded values with a coverage factor $k = 2$. MAT-RES2-NIM and MAT-RES3-NIM were not measured at NIM because these samples were seriously damaged when received by NIM.

Table 36: Measurement results of the relative permittivity and loss tangent of MAT.RES1-NIM (COP)

Laboratory	Frequency (GHz)	ϵ_r	$U(\epsilon_r)$	$\tan \delta$	$U(\tan \delta)$	Method	Direction
NIM	25.42500	2.3350	0.0150	0.00033	0.00009	SCR	In-plane
NMIJ (measurements before sending the samples to KRISS)	23.18130	2.3215	0.0085	0.00033	0.00004	SCR	In-plane
	15.84008	2.3302	0.0081	0.00028	0.00020	BCDR	Perpendicular
	29.19266	2.3275	0.0121	0.00035	0.00006		
	42.54263	2.3265	0.0149	0.00034	0.00006		
	55.92447	2.3259	0.0168	0.00036	0.00004		
69.32023	2.3255	0.0179	0.00036	0.00003			
NMIJ (measurements after returning the samples from KRISS)	23.18078	2.3226	0.0085	0.00033	0.00004	SCR	In-plane
	15.84008	2.3302	0.0081	0.00028	0.00020	BCDR	Perpendicular
	29.19266	2.3275	0.0121	0.00035	0.00006		
	42.54263	2.3265	0.0149	0.00034	0.00006		
	55.92447	2.3259	0.0168	0.00036	0.00004		
	69.32023	2.3255	0.0179	0.00036	0.00003		

6.4 Discussions

Regarding the comparison between KRISS and NMIJ, the measurement results of both laboratories using the SCR method are almost consistent for MAT.RES3-KRISS (see Fig. 11(a)). However, for low-permittivity samples of MAT.RES1-KRISS and MAT.RES2-KRISS, the results of KRISS are larger than those of NMIJ for both relative permittivity and loss tangent (see Fig. 11(a) and (b)). Although the origin of the deviations is not clear, they may be attributable to the smaller sample sizes than the specification of the KRISS measurement system. The electromagnetic field is more localized inside the cavity for the measurement of MAT.RES3-KRISS having a relatively high relative permittivity, which would alleviate the effect of a finite sample size.

Regarding the comparison between NIM and NMIJ, the measurement results of MAT.RES1-NIM obtained from both laboratories are consistent within the ranges of uncertainties for both relative permittivity and loss tangent.

The measurement results of NMIJ by using the BCDR method are consistent with those obtained using the SCR method for the relative permittivity of the COP samples (MAT.RES1-KRISS and MAT.RES1-NIM) and the loss tangent of all samples. However, there are discrepancies in the relative permittivity results of the glass samples (MAT.RES2-KRISS and MAT.RES3-KRISS). This can be partly attributed to the anisotropy of these samples. Sample surface roughness is also a possible factor. In the BCDR method, the relative permittivity would be underestimated if there is an air gap between the metal and the sample, for example due to surface roughness.

The measurement results obtained at NMIJ before and after the sample transportation are almost the same for both the SCR and BCDR methods, which confirms that the sample characteristics were almost not changed during the transportation. However, brittle glass samples that were broken during the transportation posed challenges for future comparisons in terms of sample selection and sample packaging methods for transportation.

7 Conclusions

A CCEM Pilot Study on complex permittivity measurements was conducted to verify the equivalence of permittivity measurements between NMIs. In the pilot study, one high-loss and three low-loss material samples were measured using the waveguide T/R and resonator methods, respectively, at five participating laboratories. Based on the comparison of the measurement results, no significant deviations in the measurements of the participating laboratories were identified. The changes in the properties of the acrylic samples for the TR method during the comparison and the breakage of some of the glass samples for the resonator methods provided significant information for considering future comparison protocols.

8 References

- [1] J. Baker-Jarvis, "Transmission/reflection and short-circuit line permittivity measurements," Nat. Inst. Standards Technol., Gaithersburg, MD, USA, Tech. Rep. 1341, 1990.
- [2] R. N. Clarke, Ed., "A guide to the characterisation of dielectric materials at RF and microwave frequencies," Inst. Meas. Control/Nat. Phys. Lab., Tech. Rep., 2003.
- [3] J. Krupka, A. Gregory, O. Rochard, R. Clarke, B. Riddle, and J. Baker-Jarvis, "Uncertainty of complex permittivity measurements by split-post dielectric resonator technique," *J. Eur. Ceram. Soc.*, vol. 21, no. 15, pp. 2673–2676, 2001.
- [4] M. D. Janezic, E. F. Kuester, and J. B. Jarvis, "Broadband complex permittivity measurements of dielectric substrates using a split-cylinder resonator," in *IEEE MTT-S Int. Microw. Symp. Dig.*, Jun. 2004, pp. 1817–1820 vol. 3.
- [5] J. Krupka, "Frequency domain complex permittivity measurements at microwave frequencies," *Meas. Sci. Technol.*, vol. 17, no. 6, pp. R55–R70, 2006.
- [6] Y. Kato, M. Horibe, M. Ameya, S. Kurokawa, and Y. Shimada, "New uncertainty analysis for permittivity measurements using the transmission/reflection method," *IEEE Trans. Instrum. Meas.*, vol. 64, no. 6, pp.

1748–1753, Jun. 2015.

[7] Y. Kato and M. Horibe, “Comparison of calculation techniques for Q-factor determination of resonant structures based on influence of VNA measurement uncertainty,” *IEICE Trans. Electron.*, vol. E97-C, no. 6, pp. 575–582, 2014.

[8] H. Kawabata and Y. Kobayashi, “The analysis of a balanced-type circular disk resonator excited by coaxial cable lines to measure the complex permittivity,” in *2001 Asia-Pacific Microwave Conference*, Taipei, Taiwan, Dec 2001, pp. 1322–1325 vol.3.

[9] H. Kawabata, K. i. Hasuike, Y. Kobayashi, and Z. Ma, “Multi-frequency measurements of complex permittivity of dielectric plates using higher- order modes of a balanced-type circular disk resonator,” in *2006 European Microwave Conference*, Manchester, UK, Sept 2006, pp. 388–391.

[10] Y. Kato and M. Horibe, “Permittivity measurements and associated uncertainties up to 110 GHz in circular-disk resonator method,” in *2016 European Microwave Conference*, London, UK, Oct 2016, pp. 1139–1142.

[11] Y. Kato and M. Horibe, “Broadband permittivity measurements up to 170-ghz using balanced-type circular-disk resonator excited by 0.8-mm coaxial line,” *IEEE Trans. Instrum. Meas.*, vol. 68, no. 6, pp. 1796–1805, 2019.